tvst

Article

# A Novel Approach to Quantitative Evaluation of Outer Retinal Lesions Via a New Parameter "Integral" in Spectral Domain Optical Coherence Tomography

**Junxiang Gu[1–3,*], Tingting Jiang[1–3,*], Mingrong Yu[1–3], Jian Yu[1–3], Wenting Li[4], Shixue Liu[4], Peijun Zhang[1–3], Wenwen Chen[1–3], and Qing Chang[1–3]**

[1] Department of Ophthalmology, Eye and ENT Hospital of Fudan University, Fudan University, Shanghai, China
[2] Shanghai Key Laboratory of Visual Impairment and Restoration, Eye and ENT Hospital of Fudan University, Fudan University, Shanghai, China
[3] Key NHC Laboratory of Myopia (Fudan University), Key Laboratory of Myopia, Chinese Academy of Medical Sciences, Shanghai, China
[4] Shanghai Medical College, Fudan University, Shanghai, China

**Correspondence:** Qing Chang, Department of Ophthalmology, Eye and ENT Hospital of Fudan University, Fudan University, 83 Fenyang Road, Shanghai, China 200031. e-mail: qngchang@aliyun.com

**Received:** May 10, 2020
**Accepted:** October 3, 2020
**Published:** November 2, 2020

**Keywords:** spectral domain optical coherence tomography; outer retinal lesion; ellipsoid zone; interdigitation zone

**Citation:** Gu J, Jiang T, Yu M, Yu J, Li W, Liu S, Zhang P, Chen W, Chang Q. A novel approach to quantitative evaluation of outer retinal lesions via a new parameter "integral" in spectral domain optical coherence tomography. Trans Vis Sci Tech. 2020;9(12):8, https://doi.org/10.1167/tvst.9.12.8

**Purpose:** The purpose of this study was to design a new parameter "integral" to quantitatively evaluate the spatial cumulative reflectivity of the outer retinal layers in optical coherence tomography (OCT), and to investigate its role in the detection of outer retinal diseases.

**Methods:** This was a cross-sectional study. Fovea-centered line OCT scans were performed on 60 eyes of 60 healthy volunteers and 44 eyes of 44 patients diagnosed with outer retinal diseases. The integrals of the ellipsoid zone (EZ) and interdigitation zone (IZ) were measured by respectively accumulating the grayscale values of all the pixels within the EZ and IZ at specified locations on the scanning lines, and were then adjusted by calculating their percentages on the outer retina. The integrals of the EZ and IZ were compared between the two groups.

**Results:** The integrals of the EZ and IZ were stably and normally distributed in the healthy eyes, and were significantly lower in eyes with outer retinal lesions than in healthy ones ($P < 0.05$). Moreover, the integrals of the EZ and IZ were correlated with best corrected visual acuity (BCVA; adjusted $R^2 = 0.620$) and the presence of outer retinal lesions (Nagelkerke $R^2 = 0.767$). The area under the receiver operating characteristic (ROC) curve was 0.954 (95% confidence interval [CI] = 0.918–0.990) when the integral was selected as a diagnostic variable.

**Conclusions:** Obtained from this novel quantification method, the new parameter integral was comparable between different individuals and had the potential to detect outer retinal abnormalities in reflectivity through OCT.

**Translational Relevance:** Our work verified the feasibility of the new image analysis technique in the detection of the diseases affecting the outer retina.

## Introduction

Optical coherence tomography (OCT) has been one of the most widely used noninvasive examinations since its introduction to ophthalmology. Spectral domain OCT (SD-OCT) is a widely accepted technique featuring high scanning speed and resolution, which is able to provide excellent transverse images of the retina[1] and promote qualitative diagnosis in different kinds of diseases.[2–4] Based on the improved image quality, efforts have been made to acquire quantitative information from OCT for better diagnostic accuracy. Several promising quantitative biomarkers have been found, including thickness,[5,6] structural changes,[7,8] volume,[9–11] and reflectivity.[12–14]

Outer retinal lesions can be observed in various diseases affecting the photoreceptors and lead to

poor visual outcomes.[15,16] Although some occult outer retinal lesions might not exhibit structural changes recognizable to the naked eye in OCT images. Hence, researches on the accurate evaluation have been conducted and the correlation between the photoreceptors and the outer retinal bands in OCT has been revealed.[13,17] However, the reflectivity of SD-OCT bears great variation, which makes it hard to be applied directly to the disease screening. Factors, including opacity of dioptric media, image quality, and incident angle of the light source, can largely affect the reflectivity, thus concealing the slight decreases in reflectivity caused by outer retinal diseases.[18] Therefore, improved quantification methods with better sensitivity and stability remain to be explored.

In this study, we established a novel quantification method to comprehensively evaluate the spatial cumulative reflectivity through SD-OCT by accumulating the reflectivity over the full-thickness of the target layer, the result of which was termed as "integral" according to the mathematical concept. We further assessed the data distribution of this parameter in healthy eyes, and then preliminarily evaluated its role in the detection of outer retinal disruptions.

## Methods

This was a single-centered cross-sectional study. The study was approved by the Institutional Review Board (IRB) of the Eye and ENT Hospital of Fudan University. Informed consent was obtained from the subjects, and all the examinations and researches were conducted in accordance with the Declaration of Helsinki.

### Participants

The medical data of both the healthy volunteers and the patients with outer retinal conditions were reviewed. Healthy volunteers from our database were enrolled as the normal group if the best-corrected visual acuity (BCVA) was no worse than 16/20 meanwhile the spherical equivalence was between +1 and –3D, and excluded in case of history of ocular surgery, trauma, posterior scleral staphyloma, or other ophthalmic diseases affecting the outer retinal structures. Patients referred to the Eye and ENT Hospital of Fudan University from January 2018 to December 2019 and diagnosed with inflammatory or dystrophic conditions featuring the disruption of the outer retinal layers at the fovea were included in the disease group; the exclusion criteria included the lack of fixation for a fovea-centered OCT scan, severe opacification of the refractive medium (e.g. corneal edema, severe keratic precipitates, pupillary fibrin membrane, secondary cataract, or inflammatory vitreous haze) or posterior scleral staphyloma affecting the imaging of the perifoveal region. All the participants were unilaterally included. For healthy volunteers, the laterality was determined alternatively according to the inclusion sequence. For bilaterally involved patients, the initially involved eyes were included.

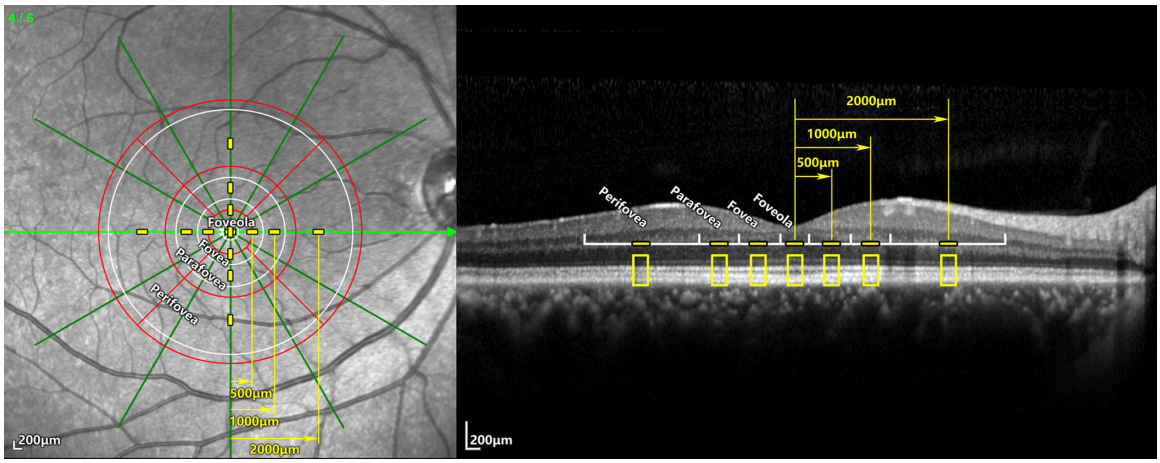


**Figure 1. Positions of the sampling areas and their relations with the anatomic regions and ETDRS grid.** Left: The infrared reflectance imaging of a radial scan; a horizontal scan and a vertical scan were selected for analysis in each eye. Right: The B-scan image of the horizontal scan. The *white circles and scales* showed the boundaries of the foveola, fovea, parafovea, and perifovea, respectively. On the 2 selected scanning lines, sampling areas 200 μm in width (*yellow line segments*) were set at different radiuses including 0, 500, 1000, and 2000 μm representing the corresponding regions. The ETDRS grid (*red*) was also marked as reference.

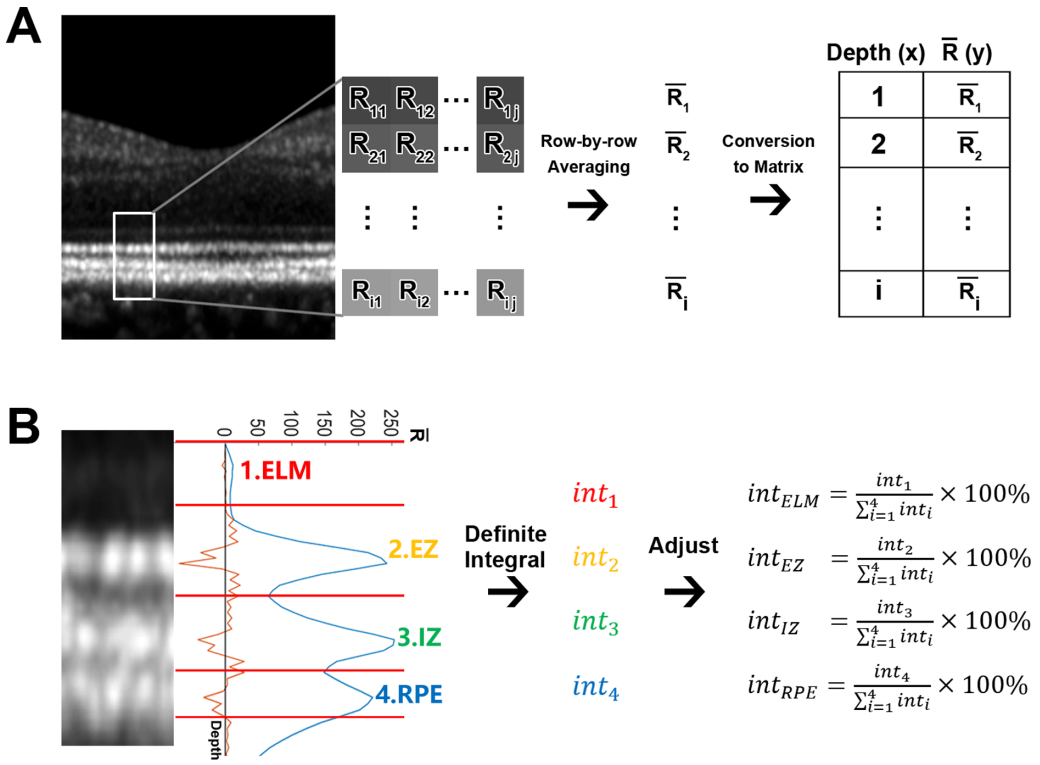


**Figure 2.** **Integral measurement of the four outer retinal layers.** (**A**) At each sampling area, the grayscale value of each pixel was read as its reflectivity. The reflectivities of each row of pixels were averaged and converted into a matrix along with its corresponding depth. (**B**) The reflectivity curve (*blue curve*) was plotted according to the matrix and the boundaries (*red lines*) were set at the troughs between the ONL, ELM, EZ, IZ, and RPE. The lower boundary of RPE was set at the inflection point on the descending slope according to the second derivative curve (*orange curve*). The original integral of each numbered layer was calculated as the AUC of the corresponding peak through definite integral, and was then divided by the sum of the four layers in order to get the adjusted integral for further analysis. Abbreviation: R, the reflectivity value of the pixel; R̄, the average reflectivity value of this row of pixels; int, integral; ONL, outer nuclear layer; ELM, external limiting membrane; EZ, ellipsoid zone; IZ, interdigitation zone; RPE, retinal pigment epithelium.

## Clinical Examinations

Basic ophthalmic information, including refraction, BCVA, and axial length, was collected. OCT images were acquired using SD-OCT (Spectralis HRA + OCT, software version 6.9; Heidelberg Engineering, Heidelberg, Germany). The scan field was 30 degrees × 30 degrees centered on the fovea; horizontal and vertical line scans across the fovea were performed at the automatic real time (ART) level of 100 frames, if possible, in order to minimize the interference of noise.

## Locations of the Sampling Areas

In the horizontal and vertical scans of each eye, sampling areas were selected for quantitative analysis in the four directions (superior, inferior, nasal, and temporal) on the two crossed scanning lines; the radiuses of the sampling areas from the center of the fovea were 0, 500, 1000, and 2000 µm representing various anatomical regions, including the foveola, fovea, parafovea, and perifovea, respectively. Each sampling area was 200 µm in width along the scanning line. Thereupon, the foveolar region contained two orthogonal sampling areas on the intersection of the two scanning lines; each of the foveal ring, parafoveal ring, and perifoveal ring contained four sampling areas in the four directions (superior, inferior, temporal, and nasal; Fig. 1).

## Protocol for Quantitative Measurement

At each sampling area, the average grayscale values of each row of pixels were read using ImageJ (http://imagej.nih.gov/ij/; provided in the public domain by the National Institutes of Health, Bethesda, MD, USA) and saved as a matrix along with the depth of this pixel row. The matrix was then imported to Matlab (MathWorks, Natick, MA, USA) and the grayscale curve was plotted (Fig. 2A).

The peaks of the four hyper-reflective layers, including the external limiting membrane (ELM),

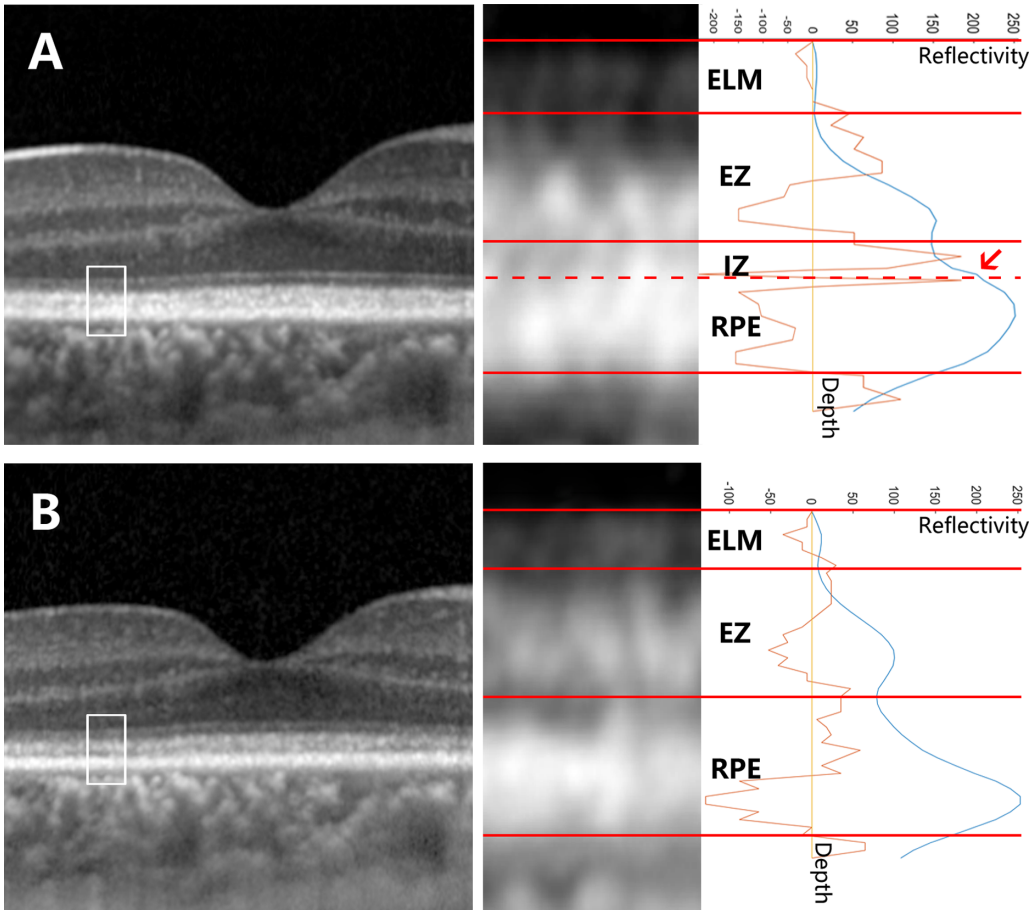


**Figure 3. Example of the segmentation in the eyes with fusion or absence of specific layers.** The OCT images of a patient with RP1L1 mutation at the first visit (**A**) and a follow-up visit 1 year later (**B**) were analyzed. **A** A fused waveform of the IZ and RPE was observed at the parafoveal sampling area. On the reflectivity curve (*blue curve*), a process (*arrow*) appearing between the EZ peak and the RPE peak generated two additional inflection points according to the second derivative curve (*orange curve*); the latter inflection point was recognized as the boundary between the IZ and the RPE (*dashed line*). **B** There was no additional inflection point between the EZ peak and the RPE peak. In this circumstance, the IZ peak was considered missing. Abbreviations: ELM, external limiting membrane; EZ, ellipsoid zone; IZ, interdigitation zone; RPE, retinal pigment epithelium.

ellipsoid zone (EZ), interdigitation zone (IZ) and retinal pigment epithelium/Bruch's complex (RPE) were segmented at the troughs between the outer nuclear layer (ONL) and ELM, between the ELM and EZ, between the EZ and IZ, and between the IZ and RPE. Because no trough could be observed between the RPE and choriocapillaris due to their tight attachment, the lower boundary of the RPE was set at the inflection point of the descending slope (see Fig. 2B). In a normal waveform, there would be two inflection points between each two adjacent crests, of which one was on the descending slope of the former peak and the other is on the ascending slope of the latter peak. Although, in case of fused or absent layers, the number of the crests and the inflection points between them would be changed. The additional inflection point was set as the boundaries between the two fused waveforms; the peak was considered absent when the crest was undetectable and no additional inflection point was observed (Fig. 3).

The beginning of the ELM peak was set as the origin of the coordinate system in order to adjust background noise and white balance. The area under the curve (AUC) of each peak was computed using definite integral and recorded as the original integral of the corresponding layer. The original integral was then self-adjusted by calculating its percentage-ratio to the total integral of the four outer retinal layers at this sampling area (see Fig. 2B). For each region, the integral values at all the sampling areas within it were averaged before further analysis.

**Table 1.** Demographic and Ophthalmic Data of the Participants

| Characteristic | Normal Group ($n = 60$) | Disease Group ($n = 44$) | *P* Value |
|---|---|---|---|
| **Demographic** | | | |
| Age (median (IQRs), year) | 42.5 (24.0 to 49.0) | 41.0 (28.5 to 52.0) | 0.625 |
| Gender (male/female) | 25/35 | 18/26 | 0.938 |
| **Ophthalmic** | | | |
| Refractive diopter (median (IQR), D) | −0.375 (−1.50 to 0.00) | −0.25 (−0.875 to 0.25) | 0.297 |
| BCVA (median (IQR), LogMAR) | 0.0 (−0.1 to 0.0) | 0.4 (0.2 to 0.5) | < 0.001 |

IQR, interquartile range; D, diopter; BCVA, best-corrected visual acuity; LogMAR, logarithm of the minimum angle of resolution.

## Statistical Analysis

All the BCVA measurements were converted to logarithm of the minimum angle of resolution (logMAR) equivalents. Wilcoxon rank sum test and Pearson $\chi^2$ test were used in the comparison of demographic features. Statistical tests were conducted as follows. (1) To explore the distribution characteristics of the integral in healthy eyes, Kolmogorov-Smirnov tests were performed to test the normality. (2) *T*-tests were performed to compare the integrals of the EZ and IZ between the normal group and the disease group. (3) The correlation of the EZ and IZ with BCVA and the presence of outer retinal lesions were analyzed using backward multiple linear regression and binary logistic regression, respectively. The predicted probability was calculated from the binary logistic regression as a comprehensive index of the correlated measurements. To preliminarily evaluate the discernibility of integral, the receiver operating characteristic (ROC) curve of the predicted probability was plotted and analyzed.

The sample size was estimated at the level of $\alpha = 0.05$ (2-sided) and 1-$\beta = 0.9$ with the POWER procedure of SAS version 9.4 (SAS Institute Inc., Cary, NC, USA). Minimal estimated sample sizes were 36 for each group and 86 for the regression based on the pre-test. Statistical analyses were carried out with SPSS version 22.0 (SPSS Inc., Chicago, IL, USA). The $P$ values $< 0.05$ were considered statistically significant.

# Results

Sixty eyes of 60 healthy volunteers were included in the normal group; 44 eyes of 44 patients were included in the disease group. The median (interquartile range [IQR]) ages of the normal group and disease group were 42.5 (24.0 to 49.0) and 41.0 (28.5 to 52.0) years, respectively. The differences in age (Wilcoxon rank sum test, $P = 0.652$), gender (Pearson $\chi^2$ test, $P = 0.938$), and refraction status (Wilcoxon rank sum test, $P = 0.297$) were of no statistical significance between the two groups; the logMAR visual acuity was 0.0 (−0.1 to 0.0) and 0.4 (0.2 to 0.5), respectively (Wilcoxon rank sum test, $P < 0.001$; Table 1). Disease distribution of the disease group is detailed in Table 2.

Ninety-five subjects (91.3%), including 60 healthy volunteers and 35 patients, accomplished OCT scans with the ART of 100 frames, whereas the images of 9 patients (8.7%) were captured with the ART of 30 frames. Lower ART did not affect the measurement of integral (data not shown).

As to the segmentation of the outer retina, fusion and absence of the EZ or IZ were observed in 26 eyes (25.0%) from the disease group, among which there were 11 eyes (10.6%) with fused waveforms, 10 eyes (9.6%) with absent waveforms, and 5 eyes (4.8%) with both. All the 26 eyes fitted the predefined segmentation strategy.

## Data Distribution of Integral in Health Eyes

The normal group ($n = 60$ eyes) were enrolled for the analysis on the data distribution of the integral values. Kolmogorov-Smirnov tests indicated that the average integrals of the EZ, IZ, and RPE at all the four regions (foveola, fovea, parafovea, and perifovea) were normally distributed (Table 3).

## Comparison of Integral between Healthy Eyes and Eyes with Outer Retinal Lesions

The normal group and the disease group were enrolled ($n = 104$ eyes); the integrals of the EZ and IZ were compared between the two groups. The integrals of the EZ and IZ were significantly lower in the disease

**Table 2.** Disease Distribution of the Disease Group

| Disease | Patient ($n = 44$) | Percentage |
|---|---|---|
| **Non-infectious inflammation** | **21** | |
| White dot syndrome | 5 | 11% |
| Cancer-associated retinopathy | 3 | 7% |
| Uveitis | 13 | 30% |
| **Infectious uveitis** | **13** | |
| Tuberculosis | 9 | 20% |
| Syphilis | 4 | 9% |
| **Retinal dystrophy** | **10** | |
| Retinitis pigmentosa | 7 | 16% |
| Cone-rod dystrophy | 1 | 2% |
| Occult macular dystrophy | 2 | 5% |

**Table 3.** Medians, Means, and Normality Test Results of the Integral Values in the Healthy Group

| Layer | Region | Median (IQR) (%) | Normality[a] | Mean ± SD (%) |
|---|---|---|---|---|
| **ELM** | Foveola | 2.4 (2.0–3.1) | $P < 0.001$ | / |
| | Fovea | 2.6 (2.1–3.1) | $P = 0.001$ | / |
| | Parafovea | 1.9 (1.6–2.5) | $P = 0.018$ | / |
| | Perifovea | 1.6 (1.3–1.9) | $P = 0.001$ | / |
| **EZ** | Foveola | 27.7 (24.5–30.1) | $P > 0.200$ | 27.4 ± 4.2 |
| | Fovea | 31.1 (28.1–34.0) | $P > 0.200$ | 31.1 ± 4.2 |
| | Parafovea | 34.7 (31.3–38.1) | $P > 0.200$ | 34.7 ± 4.6 |
| | Perifovea | 34.0 (31.6–36.1) | $P > 0.200$ | 34.0 ± 4.2 |
| **IZ** | Foveola | 34.4 (30.5–38.2) | $P > 0.200$ | 35.0 ± 7.0 |
| | Fovea | 38.6 (35.4–42.1) | $P > 0.200$ | 38.5 ± 5.2 |
| | Parafovea | 36.4 (32.9–39.2) | $P > 0.200$ | 36.5 ± 5.3 |
| | Perifovea | 29.9 (27.0–33.9) | $P > 0.200$ | 30.2 ± 5.7 |
| **RPE** | Foveola | 36.3 (29.3–40.2) | $P = 0.195$ | 34.8 ± 8.3 |
| | Fovea | 27.0 (23.8–30.0) | $P > 0.200$ | 27.6 ± 4.8 |
| | Parafovea | 26.1 (22.6–30.0) | $P > 0.200$ | 26.7 ± 5.0 |
| | Perifovea | 33.6 (30.0–38.3) | $P > 0.200$ | 34.1 ± 6.5 |

[a] *P* value of the Kolmogorov-Smirnov test.

IQR, interquartile range; SD, standard deviation; ELM, external limiting membrane; EZ, ellipsoid zone; IZ, interdigitation zone.

group than in the normal group (*t*-test, $P < 0.05$; Table 4).

## Correlation of Integral with BCVA and the Presence of Outer Retinal Lesions

Tested by the backward multiple linear regression, the integrals of the EZ at the parafovea, and IZ at the fovea and parafovea were correlated with BCVA ($P < 0.001$, $P = 0.024$, and $P = 0.024$, respectively; adjusted $R^2 = 0.620$). The binary logistic regression showed that the integrals of the EZ at the parafovea and IZ at the parafovea were correlated with the presence of outer retinal lesions ($P = 0.007$ and $P < 0.001$, respectively, Nagelkerke $R^2 = 0.767$;(Table 4).

The predicted probability of each eye was obtained from the binary logistic regression as a diagnostic index of outer retinal lesions. The ROC curves were plotted. The AUC of the ROC curve was 0.954 (95% confidence intervals [CIs] = 0.918–0.990). The sensitivity was 84.1% and the specificity was 95.0% when the Youden index reached the maximum of 0.791 (Fig. 4).

## An Example of the Application of Integral in the Evaluation of Outer Retinal Lesions

A female patient aged 28 years presented with declined visual acuity in both eyes (BCVA = OD 20/32 and OS 20/50) and was afterward diagnosed with occult macular degeneration caused by RP1L1

**Table 4.** Comparison of the Integrals Between the Normal Group and the Disease Group, and the Statistical Results of the Regression Tests for the Correlation With BCVA and Presence of Outer Retinal Lesions

| Layer | Region | Normal Group Mean ± SD (%) | Disease Group Mean ± SD (%) | *t*-test | Regression | |
|---|---|---|---|---|---|---|
| | | | | | Linear[a] | Logistics[b] |
| **EZ** | Foveola | 27.4 ± 4.2 | 21.5 ± 8.6 | $P < 0.001$ | $P = 0.698$ | $P = 0.075$ |
| | Fovea | 31.1 ± 4.2 | 26.9 ± 9.0 | $P = 0.006$ | $P = 0.419$ | $P = 0.971$ |
| | Parafovea | 34.7 ± 4.6 | 27.0 ± 9.6 | $P < 0.001$ | $P < 0.001$ | $P = 0.007$ |
| | Perifovea | 34.0 ± 4.2 | 26.5 ± 11.1 | $P < 0.001$ | $P = 0.233$ | $P = 0.107$ |
| **IZ** | Foveola | 35.0 ± 7.0 | 22.0 ± 13.8 | $P < 0.001$ | $P = 0.053$ | $P = 0.632$ |
| | Fovea | 38.5 ± 5.2 | 22.7 ± 12.2 | $P < 0.001$ | $P = 0.024$ | $P = 0.598$ |
| | Parafovea | 36.5 ± 5.3 | 19.5 ± 10.4 | $P < 0.001$ | $P = 0.024$ | $P < 0.001$ |
| | Perifovea | 30.2 ± 5.7 | 17.6 ± 10.0 | $P < 0.001$ | $P = 0.279$ | $P = 0.796$ |

[a]*P* values of the multiple linear regression. The dependent variable was the LogMAR equivalent of BCVA.

[b]*P* values of the binary logistics regression. The dependent variable was a binary variable representing whether the eye had outer retinal lesions.

EZ, ellipsoid zone; IZ, interdigitation zone; BCVA, best corrected visual acuity.

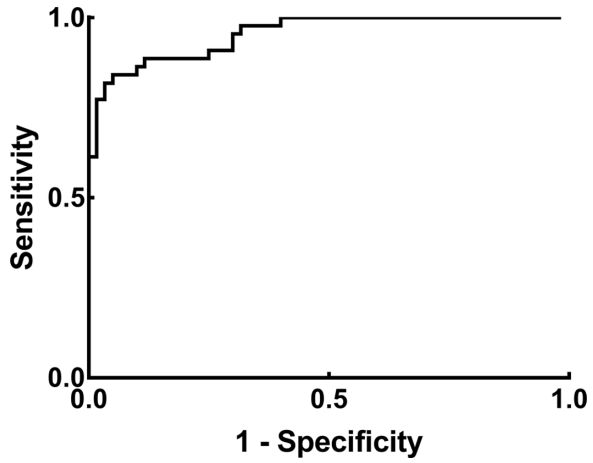


**Figure 4. The ROC curve when the integrals of the EZ and IZ were used to detect outer retinal lesions.** The predicted probability was calculated from the binary logistic regression as a comprehensive index of the EZ and IZ. The AUC of the ROC curve was 0.954 (95% CI = 0.918–0.990) when the predicted probability was used to detect outer retinal lesions. Abbreviations: ROC curve, receiver operating characteristic curve; AUC, area under curve; 95% CI, 95% confidence interval.

mutation. To take the right eye as an example, the OCT at the first visit revealed the blurring of the IZ (see Fig. 3A), the integral of which at the temporal foveal sampling area (value = 20.5%) was below the lower limit of the 95% CI (threshold = 28.3%; see Table 3) at the corresponding region of the healthy eyes, whereas the integral of the EZ was normal (value = 26.6%). At the 1-year follow-up, the visual acuity continued to decrease (BCVA = OD 20/100 and OS 20/100). The OCT showed the absence of the IZ and the blurring of the EZ (see Fig. 3B). At the same sampling area, the integral of the EZ (value = 20.0%) fell below the lower limit of the 95% CI (threshold = 22.9%; see Table 3) in healthy eyes, which indicated the progression of the outer retinal impairment.

## Discussion

In our study, we established an efficient method to quantitatively evaluate the outer retinal layers in OCT images through a new parameter, "integral," which was calculated by accumulating the reflectivity of the full-thickness layer in a selected sampling area, and was thus able to reflect the spatial cumulative reflectivity of the target layer. In addition, we preliminarily verified its capability of detecting retinal abnormalities in patients with outer retinal reflectivity abnormalities.

Outer retinal layers in OCT images had long been considered as the predictor of visual prognosis in various diseases due to its correspondence with the anatomic layer as photoreceptors.[17] Previous studies demonstrated the relation between the EZ and visual acuity in different kinds of diseases involving the macula.[19–21] In our study, significant decreases in the integrals of the EZ and IZ were observed in the eyes with outer retinal lesions, which was consistent with previous literatures. Further regional analyses indicated that the integrals of the EZ and IZ at the foveola were not as well correlated with BCVA and the presence of outer retinal lesions as those at the parafovea (see Table 4). One possible explanation was that the innermost fovea would be less affected than the parafovea in the included patients due to the criterion of good fixation for fovea-centered scans. However, the

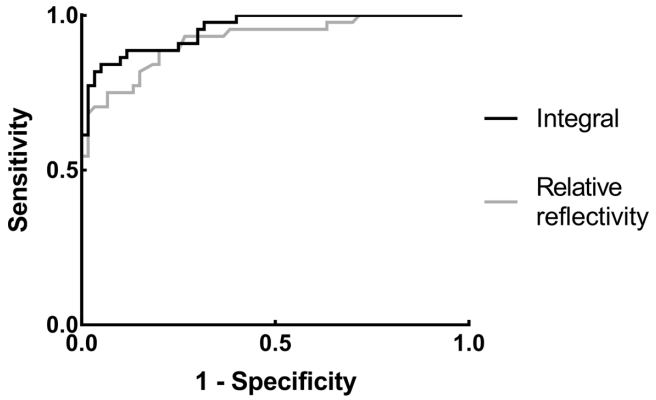


**Figure 5. Comparison between integral and an existing parameter as diagnostic tests in the detection of outer retinal lesions.** We compared integral (*black curve*) with another existing parameter measuring the relative reflectivity to the RPE (*gray curve*). The sensitivity, specificity, Youden index, and AUC of ROC curve were 84.1%, 95.0%, 0.791, and 0.954 for integral, and 80.0%, 88.6%, 0.686, and 0.921 for relative reflectivity. Abbreviations: ROC curve, Receiver operating characteristic curve; AUC, area under curve.

direct comparison between the two groups through *t*-test still showed an extensive decline in the EZ and IZ at all the four regions, which indicated that a thorough evaluation of the entire macula would still be necessary.

Generated by the mitochondria and interdigitated outer segment, the reflectivity of the EZ and IZ in OCT images were closely correlated with the energy production and density of the photoreceptors.[13,17] Previously, the relative peak reflectivity of the EZ and IZ to the RPE was applied to occult macular dystrophy and exhibited good potential in the quantitative evaluation of the outer retina.[22] In order to compare our method with the existing one, we also measured the relative reflectivity in the participants. The sensitivity, specificity, Youden index, and AUC of ROC curve were 80.0%, 88.6%, 0.686, and 0.921 for relative reflectivity, and 84.1%, 95.0%, 0.791, and 0.954 for integral (Fig. 5). Besides, integral was better correlated with BCVA (adjusted $R^2 = 0.620$) and the presence of outer retina lesions (Nagelkerke $R^2 = 0.767$) than relative reflectivity (adjusted $R^2 = 0.539$ and Nagelkerke $R^2 = 0.684$). The potential advantage of integral lay in that it measured the total amount of the hyper-reflective matter (e.g. the mitochondria or the interdigitated outer segment) by integrating the reflectivity with respect to the thickness of the target layer. By contrast, the existing parameter, relative reflectivity, measured the density of the hyper-reflective matter at a particular depth without considering the thickness of the layer to be measured. Therefore, the comparison with the existing parameter indicated that integral was a feasible parameter to detect outer retinal disruptions.

Segmentation was also essential for the quantification of the outer retina. Previous literature showed that existing automated segmentation software might lead to segmentation errors when applied to diseased eyes.[23] In our study, fused or absent waveforms of the EZ or IZ were observed in 26 eyes. All these eyes fitted our predefined segmentation method based on inflection point analysis, and yielded available measurements without manual adjustment, which indicated that this segmentation strategy was feasible to evaluate these two types of abnormities.

Self-adjustment was essential for the elimination of individual differences in medical measurement. Commonly used references could be another metric (e.g. the height in the calculation of body mass index [BMI] index) or the totality of the metric being measured (e.g. the total leukocyte counts in the calculation of neutrophil percentage). In previous literatures, the RPE or the full-thickness retina was chosen as the reference for adjustment.[13,22] In our study, the total integral of the four layers (ELM, EZ, IZ, and RPE) was set as the reference. The potential benefits were as follows. First, the totality of the outer retina was less volatile than the RPE alone, thus providing better data stability. Second, our algorithm could detect RPE disorders, which the RPE-adjusted algorithm was unable to evaluate. Third, the decline in one band would lead to the rise in the proportion of the others, which could raise the numeric contrast. As a result, the integral adjusted by our algorithm had narrower IQR intervals (compared after zero-mean normalization using Wilcoxon signed ranks test, $P < 0.001$) and greater AUC of the ROC curve (0.954 vs. 0.951) than adjusted by the RPE.

The limitations of this study were as follows. (1) We only measured the integrals on the vertical and horizontal scans for the preliminary screening of macula-involved diseases. Therefore, additional customized scanning areas would be required if the lesions were not fovea-centered. (2) In this study, we mainly analyzed the conditions initially affecting the EZ and IZ (e.g. inflammatory diseases and dystrophic diseases). The distribution pattern of this parameter needed to be further explored before its application to other complicated diseases. (3) The images were imported manually to the Matlab for the calculation of integral due to the lack of in-built algorithms in the software of SPECTRALIS, which made it difficult to give instant diagnoses. (4) This was a pilot study; the feasibility of our method needed to be further tested by another prospective research in the future.

In conclusion, the new parameter, "integral," was able to yield ideal data distribution in a healthy population. The integrals of the EZ and IZ were correlated with visual acuity and the presence of outer retinal disruptions, and had the ability to detect outer retinal abnormalities through SD-OCT.

## Acknowledgments

Supported by the National Natural Science Foundation of China (Grants no. 81870670 and 81500734) and the Shanghai Committee of Science and Technology (Grant no. 18411965100).

Disclosures: **J. Gu,** None; **T. Jiang,** None; **M. Yu,** None; **J. Yu,** None; **W. Li,** None; **S. Liu,** None; **P. Zhang,** None; **W. Chen,** None; **Q. Chang,** None

* JG and TJ contributed equally to the manuscript.

## References

1. Geitzenauer W, Hitzenberger CK, Schmidt-Erfurth UM. Retinal optical coherence tomography: past, present and future perspectives. *Br J Ophthalmol*. 2011;95(2):171–177.
2. Mojana F, Cheng L, Bartsch DU, et al. The role of abnormal vitreomacular adhesion in age-related macular degeneration: spectral optical coherence tomography and surgical results. *Am J Ophthalmol*. 2008;146(2):218–227.
3. Leung CK, Lam S, Weinreb RN, et al. Retinal nerve fiber layer imaging with spectral-domain optical coherence tomography: analysis of the retinal nerve fiber layer map for glaucoma detection. *Ophthalmology*. 2010;117(9):1684–1691.
4. Comander J, Gardiner M, Loewenstein J. High-resolution optical coherence tomography findings in solar maculopathy and the differential diagnosis of outer retinal holes. *Am J Ophthalmol*. 2011;152(3):413–419.e6.
5. Pelosini L, Hull CC, Boyce JF, et al. Optical coherence tomography may be used to predict visual acuity in patients with macular edema. *Invest Ophthalmol Vis Sci*. 2011;52(5):2741–2748.
6. Ruia S, Saxena S, Prasad S, et al. Correlation of biomarkers thiobarbituric acid reactive substance, nitric oxide and central subfield and cube average thickness in diabetic retinopathy: a cross-sectional study. *Int J Retina Vitreous*. 2016;2:8.
7. Sharma S, Saxena S, Srivastav K, et al. Nitric oxide and oxidative stress is associated with severity of diabetic retinopathy and retinal structural alterations. *Clin Exp Ophthalmol*. 2015;43(5):429–436.
8. Uji A, Murakami T, Unoki N, et al. Parallelism for quantitative image analysis of photoreceptor-retinal pigment epithelium complex alterations in diabetic macular edema. *Invest Ophthalmol Vis Sci*. 2014;55(5):3361–3367.
9. Gregori G, Wang F, Rosenfeld PJ, et al. Spectral domain optical coherence tomography imaging of drusen in nonexudative age-related macular degeneration. *Ophthalmology*. 2011;118(7):1373–1379.
10. Breger A, Ehler M, Bogunovic H, et al. Supervised learning and dimension reduction techniques for quantification of retinal fluid in optical coherence tomography images. *Eye (Lond)*. 2017;31(8):1212–1220.
11. Hsu ST, Gabr H, Viehland C, et al. Volumetric measurement of subretinal blebs using microscope-integrated optical coherence tomography. *Transl Vis Sci Technol*. 2018;7(2):19.
12. Saleh M, Flores M, Gauthier AS, Elphege E, Delbosc B. Quantitative analysis of photoreceptor layer reflectivity on en-face optical coherence tomography as an estimator of cone density. *Graefes Arch Clin Exp Ophthalmol*. 2017;255(11):2119–2126.
13. Flores M, Debellemaniere G, Bully A, et al. Reflectivity of the outer retina on spectral-domain optical coherence tomography as a predictor of photoreceptor cone density. *Am J Ophthalmol*. 2015;160(3):588–595.e2.
14. Allahdina AM, Stetson PF, Vitale S, et al. Optical coherence tomography minimum intensity as an objective measure for the detection of hydroxychloroquine toxicity. *Invest Ophthalmol Vis Sci*. 2018;59(5):1953–1963.
15. Landa G, Su E, Garcia PM, Seiple WH, Rosen RB. Inner segment-outer segment junctional layer integrity and corresponding retinal sensitivity in dry and wet forms of age-related macular degeneration. *Retina*. 2011;31(2):364–370.
16. Maheshwary AS, Oster SF, Yuson RM, et al. The association between percent disruption of the photoreceptor inner segment-outer segment junction and visual acuity in diabetic macular edema. *Am J Ophthalmol*. 2010;150(1):63–67.e1.
17. Spaide RF, Curcio CA. Anatomical correlates to the bands seen in the outer retina by optical coherence tomography: literature review and model. *Retina*. 2011;31(8):1609–1619.
18. Bhende M, Shetty S, Parthasarathy MK, Ramya S. Optical coherence tomography: a guide to

interpretation of common macular diseases. *Indian J Ophthalmol*. 2018;66(1):20–35.
19. Oster SF, Mojana F, Brar M, et al. Disruption of the photoreceptor inner segment/outer segment layer on spectral domain-optical coherence tomography is a predictor of poor visual acuity in patients with epiretinal membranes. *Retina*. 2010;30(5):713–718.
20. Fang IM, Hsu CC, Chen LL. Correlation between visual acuity changes and optical coherence tomography morphological findings in idiopathic epiretinal membranes. *Graefes Arch Clin Exp Ophthalmol*. 2016;254(3):437–444.
21. Iu L, Lee R, Fan M, et al. Serial spectral-domain optical coherence tomography findings in acute retinal pigment epitheliitis and the correlation to visual acuity. *Ophthalmology*. 2017;124(6):903–909.
22. Kato Y, Hanazono G, Fujinami K, et al. Parafoveal photoreceptor abnormalities in asymptomatic patients with RP1L1 mutations in families with occult macular dystrophy. *Invest Ophthalmol Vis Sci*. 2017;58(14):6020–6029.
23. Dysli C, Enzmann V, Sznitman R, Zinkernagel MS. Quantitative analysis of mouse retinal layers using automated segmentation of spectral domain optical coherence tomography images. *Transl Vis Sci Technol*. 2015;4(4):9.